Wide-Band Guided-Wave Acoustooptic Bragg Diffraction and Devices Using Multiple Tilted Surface Acoustic Waves

CHEN S. TSAI, MEMBER, IEEE, M. A. ALHAIDER, STUDENT MEMBER, IEEE, LE TRONG NGUYEN, AND BUMMAN KIM

Abstract—Guided-wave acoustooptic Bragg diffraction from a single surface acoustic wave (SAW) and from two tilted SAW's has been analyzed to establish the design parameters of the related devices. Design and performance figures of the devices involving three and four tilted SAW's in single-mode Y-cut $LiNbO_3$ out-diffused waveguides are described in detail. Device bandwidth of up to 358 MHz, an optical throughput coupling efficiency of up to 25 percent, and very good optical beam quality have been realized. A bandwidth of 358 MHz enables the device to deflect a light beam of 1-cm aperture into 1000 resolvable spot diameters with a random-access switching time of 2.8 μs. A total electric drive power of 220 mW was required to diffract 50 percent of the incident light power for the unit with 245-MHz bandwidth. The development of this wide-band technique has paved the way for using such guided-wave acoustooptic devices in a number of applications in addition to those common to bulk-type acoustooptic devices.

I. INTRODUCTION

NONCOLLINEAR coplanar acoustooptic (AO) Bragg interaction, involving surface acoustic waves (SAW) and guided-optical waves, has been a subject of considerable interest in recent years [1]-[6]. Some of the more obvious advantages of the related guided-wave AO Bragg devices over their bulk-type counterparts are the following. 1) Since the energies of both the guided-optical waves and the SAW's are concentrated in a thin layer and also since both waves spread (by diffraction) only in one dimension, less RF drive power is required to achieve a high diffraction efficiency with the guided-wave devices. 2) The dispersion properties of both the guided-light waves and the SAW's enable the phase matching conditions to be fulfilled for a wider range of acoustic frequency and, therefore, a wider device bandwidth is inherent with guided-wave devices. 3) Guided-wave devices have smaller size and lighter weight, and have less critical isolation and alignment problems. 4) There exists a good possibility for batch fabrication of the guided-wave devices and thus for a great reduction in cost. 5) As a result of their planar configuration, the guided-wave devices are easier to fabricate and are more compatible with future fiber/integrated optic systems. Indeed, very efficient diffraction has been demonstrated in recent experiments using Y-cut $LiNbO_3$ waveguiding layers [1]-[5]. For example, a diffraction efficiency of 85 percent and a -3-dB bandwidth of 100 MHz, requiring only 190-mW electric drive power, have been demonstrated using a single SAW of 180-MHz center frequency [2d]. This efficient interaction results, not only from the fact that the frequency range of the SAW may be chosen to achieve a good matching between optical confinement and the SAW penetration depth, but also from the fact that the electrooptic effect arising from the intense piezoelectric field, which accompanies the SAW, can enhance the interaction in the Y-cut $LiNbO_3$ substrate [7].[1]

Manuscript received August 11, 1975; revised November 11, 1975. This work was supported by the NSF and the ONR.

The authors are with the Department of Electrical Engineering, Carnegie-Mellon University, Pittsburgh, PA 15213.

[1] The possibility of enhancement in diffraction efficiency due to the electrooptic effect was suggested by the authors in 1973 [7]. This enhancement was observed by investigators at IBM [4] and the authors in 1974.

However, for many potential applications involving guided-wave AO devices, bandwidth is the most important device characteristic, particularly for a number of anticipated wide-band applications to be mentioned later in this paper. For example, in beam deflection and switching applications, the wider the device bandwidth, the larger will be the number of scannable spot diameters and the faster will be the switching speed of the deflected light beam. Bandwidth of a guided-wave AO Bragg device is limited by both the acoustic bandwidth of the SAW transducer and the Bragg bandwidth. The first inherent limitation of guided-wave AO devices which employ a single interdigital transducer, and thus a single SAW, is their relatively small acoustic bandwidth. This limitation results from the fact that the fractional acoustic bandwidth is inversely proportional to the number of finger electrode pairs, while the electric–acoustic conversion efficiency is proportional to the number of finger electrode pairs squared [8]. It follows that a balance between the fractional acoustic bandwidth and the electric–acoustic conversion efficiency will automatically limit the former to a relatively small value.

With regard to the second inherent limitation on the device bandwidth, it is observed that unlike bulk-type devices [9], the Bragg bandwidth of guided-wave devices not only is limited by the acoustic center frequency, the acoustic bandwidth, and the aperture of the SAW, but also depends on the diffraction efficency of the device and the optical modes involved [2d]. While this dependence for the devices which employ Y-cut $LiNbO_3$ substrate is presented in this paper, it suffices to point out here that in order to realize a large Bragg bandwidth (assuming an acoustic bandwidth sufficiently larger than the Bragg bandwidth), the aperture of the single SAW must be chosen very small. This requirement in turn results in a drastic decrease in diffraction efficiency. Under such an unfavorable condition, a device with both large diffraction efficiency and large bandwidth requires a large RF drive power, which may easily result in the failure of the interdigital transducer. Thus it can be concluded that the diffraction efficiency–bandwidth product of a guided-wave AO device using a single SAW is rather limited.

Recently, we have experimented with two device configurations utilizing multiple SAW's—namely, tilted [2] and phased SAW's [2a], [10], [11]—in order to determine their bandwidth capability. The first device configuration employs multiple interdigital SAW transducers which are characterized by staggered center frequencies and propagation axes tilted with respect to each other. It is clear that the multiple tilted SAW's generated by such a transducer array can be made to satisfy the Bragg condition in each frequency band, and thus enable a broad composite frequency response to be realized. The second device configuration is characterized by multiple interdigital SAW transducers of identical center frequency and propagation axis, but arranged in a stepped configuration. As a result of the step height, a phase shift is introduced between adjacent SAW's, and the resultant wavefront can be scanned by varying the acoustic frequency. Scanning of the wavefront enables a composite acoustic beam of large aperture to track the Bragg condition and, therefore, make efficient diffraction possible for a relatively wide frequency band. Preliminary experimental results have borne out the above observations. For example, by employing just two tilted SAW's on a Y-cut $LiNbO_3$ out-diffused waveguide, a −3-dB bandwidth of 200 MHz with 50-percent diffraction efficiency was obtained, requiring a total electric drive power of only 200 mW [2c]. Also, by employing six-element phased SAW's, a −3-dB bandwidth of 110 MHz with 50-percent diffraction efficiency was obtained, requiring a total electric drive power of only 70 mW [11]. These performance figures greatly exceed that obtained in previous devices which employ only a single SAW.

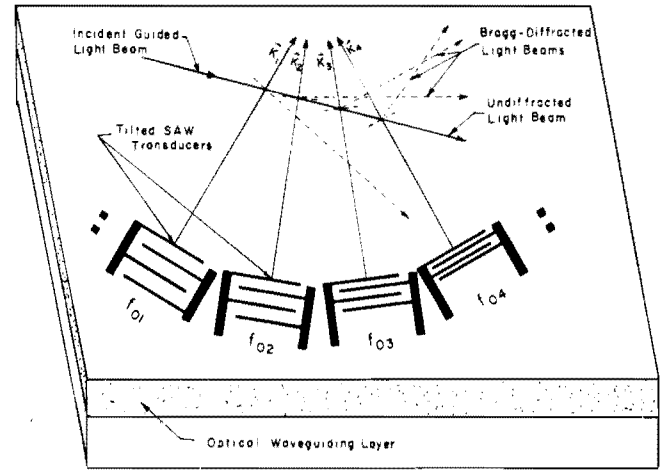

Fig. 1. Guided-wave acoustooptic Bragg diffraction from multiple tilted SAW's.

We report in this paper some theoretical and new experimental results relating to the first wide-band device configuration described above. First, the diffraction efficiency and the bandwidth of the AO Bragg diffraction using a single SAW in a Y-cut $LiNbO_3$ out-diffused optical guiding layer are analyzed in detail. The methodology for numerical computation has been established to calculate the diffraction efficiency and the bandwidth as a function of the optical and acoustic parameters such as the penetration depth of the guiding layer, waveguide modes, direction of propagation, center frequency, and aperture of the SAW. The same analytical approach and numerical computation methodology are then applied to the case of two tilted SAW's. The resultant diffraction efficiency and the bandwidth (as a function of various device parameters such as the center frequency and the beam aperture of the individual SAW's), the tilt angle, as well as the phase shift between adjacent SAW's, and the optical waveguide modes involved are calculated. Experiments using from two to four tilted SAW's in single-mode Y-cut $LiNbO_3$ out-diffused waveguides [12] were carried out to verify the theoretical predictions. In one of the wide-band units being studied, a device bandwidth of 358 MHz has been realized. A bandwidth of 358 MHz enables the device to deflect a light beam of 1-cm aperture into 1000 resolvable spot diameters at a random-access switching time of 2.8 μs. The development of this wide-band technique has paved the way for using such guided-wave AO devices for a number of wide-band applications.

II. Acoustooptic Bragg Diffraction from a Single Surface Acoustic Wave

A. Coupled-Mode Analysis

We have employed the coupled-mode approach similar to that employed by Ohmachi [1] for the analysis of noncollinear coplanar Bragg diffraction from multiple tilted SAW's (see Fig. 1). It should be noted, however, that while a step-index optical waveguide is considered in [1], a gradient-index optical waveguide is considered in this study as Y-cut $LiNbO_3$ out-diffused waveguiding layers [12] were utilized in the devices being studied. As a result, the numerical computations involved are considerably more complicated. It is also to be noted that in this study the contribution to the interaction

from the electrooptic effect which accompanies the SAW is taken into account because this contribution is important in $LiNbO_3$ substrates. However, the contribution from the surface ripple is neglected as it is small compared to the elastooptic and the electrooptic contributions.

Although our main concern is with the interaction configuration involving multiple tilted SAW's, we shall first consider the one involving only a single SAW, or equivalently, the interaction configuration involving the first SAW of multiple tilted SAW's, as the results obtained will reveal the key device parameters as well as the limitations of the devices using a single SAW. The methodology for numerical computation which is developed for the case involving a single SAW can be conveniently extended to the case involving two or more tilted SAW's. Only an outline of the analysis and some of the most relevant results will be presented in this paper. The complete analysis and results for the general case involving any number of tilted SAW's will be published elsewhere [11].

Since a Y-cut $LiNbO_3$ out-diffused waveguide can support only TE modes [12], we assume that the coplanar Bragg diffraction involves the interactions among the incident light of the mth TE mode, the diffracted light of the nth TE mode, and a piezoelectric SAW propagating in the z direction (see Fig. 2). In the following analysis, the subscript 1 designates the quantities relating the first SAW. The corresponding angles of incidence and diffraction, θ_{m1} and θ_{n1}, measured from the normal to the acoustic wave vector K_1, are determined not only by the optical and acoustic wavelengths but also by the refractive indices n_{m1} and n_{n1} for the m_1th and n_1th modes, respectively [1], [13]. Note that when there is no mode conversion between the diffracted and the undiffracted light waves, $n_1 \equiv m_1$ and $n_{n1} \equiv n_{m1}$, and thus the Bragg condition reduces to the well-known one in an isotropic medium [9].

Assuming that the medium is lossless both optically and acoustically, the corresponding electric fields $\hat{E}_{m1}$ and $\hat{E}_{n1}$ of the undiffracted and diffracted light waves, and the strain field $\hat{S}_1$ of the SAW and its accompanying piezoelectric field $\hat{E}_{p1}$ can be written as follows:

$$\hat{E}_{m1}(x,y,z,t) = 1/2E_{m1}(x)U_{m1}(y) \cdot \exp j(\omega_{m1}t - k_{m1x}x - k_{m1z}z) + \text{C.C.} \quad (1a)$$

$$\hat{E}_{n1}(x,y,z,t) = 1/2E_{n1}(x)U_{n1}(y) \cdot \exp j(\omega_{n1}t - k_{n1x}x - k_{n1z}z) + \text{C.C.} \quad (1b)$$

$$\hat{S}_1(y,z,t) = 1/2S_{I1}U_{aI1}(y) \exp j(\Omega_1 t - K_1 z + \phi_1) + \text{C.C.}, \quad I = 1,2,3,4,5,6 \quad (1c)$$

$$\hat{E}_{p1}(y,z,t) = 1/2E_{pi1}U_{pi1}(y) \exp j(\Omega_1 t - K_1 z + \phi_1) + \text{C.C.}, \quad i = 1,2,3 \quad (1d)$$

where $E_{m1}(x)$ and $E_{n1}(x)$ are the spatial distribution of the undiffracted and diffracted light waves to be determined; S_{I1} and E_{pi1} are the components of the strain field and its accompanying piezoelectric field, respectively. $U_{m1}(y)$, $U_{n1}(y)$, $U_{aI1}(y)$, and U_{pi1} are, respectively, the normalized field distribution (along the waveguide thickness) of the light waves, the acoustic wave, and the piezoelectric field. It is to be noted that for simplicity the subscripts I and i will be dropped henceforth. The frequencies of the light waves and the acoustic wave are designated by ω_{m1}, ω_{n1}, and Ω_1, respectively. Similarly, k_{m1}, k_{n1}, and K_1 designate the corresponding wavenumbers

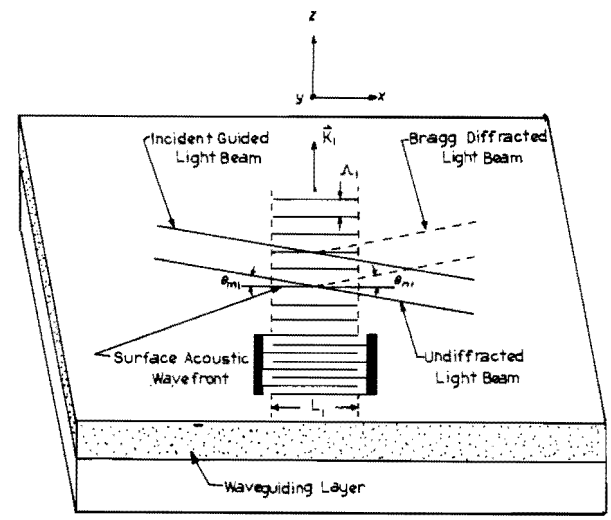

Fig. 2. Guided-wave acoustooptic Bragg diffraction from a single SAW.

and the suffixes x and z represent the x and z components. Finally, ϕ_1 designates the phase of the SAW.

When (1a), (1b), (1c), and (1d) are substituted into the wave equation for the electric field of the optical waves, a set of coupled wave equations for $E_{m1}(x)$ and $E_{n1}(x)$ are obtained. These coupled wave equations are then readily reduced to the following decoupled form:

$$\frac{\partial^2 E_{m1}(x)}{\partial x^2} - jK_1\Delta\theta_1 \frac{\partial E_{m1}(x)}{\partial x} + A_1B_1E_{m1}(x) = 0 \quad (2a)$$

$$\frac{\partial^2 E_{n1}(x)}{\partial x^2} + jK_1\Delta\theta_1 \frac{\partial E_{n1}(x)}{\partial x} + A_1B_1E_{n1}(x) = 0. \quad (2b)$$

From (2a) and (2b), general solutions for $E_{m1}(x)$ and $E_{n1}(x)$ are easily found. By matching the boundary conditions $E_{m1}(0) \equiv 1$ and $E_{n1}(0) \equiv 0$ to these general solutions, the electric field of the undiffracted and diffracted light waves at the output of the interaction region ($x = L_1$) are given as follows:

$$E_{m1}(L_1) = \{\cos(q_1L_1) - j(K_1\Delta\theta_1/2q_1)\sin(q_1L_1)\} \cdot \exp j(K_1\Delta\theta_1L_1/2) \quad (2c)$$

$$E_{n1}(L_1) = j(B_1/q_1)\sin(q_1L_1)\exp j\{-(K_1\Delta\theta_1L_1/2) + \phi_1\} \quad (2d)$$

where

$$q_1^2 \equiv (K_1\Delta\theta_1/2)^2 + A_1B_1 \quad (2e)$$

$$A_1 \equiv \frac{\omega_{n1}^2 n_{m1}^2 n_{n1}^2}{4c^2 k_{m1}\cos\theta_{m1}} \left\{P_1S_1\int_0^\infty U_{m1}U_{n1}U_{a1}\,dy + r_1E_{p1} \cdot \int_0^\infty U_{m1}U_{n1}U_{p1}\,dy\right\} \Big/ \int_{-\infty}^\infty U_{m1}^2\,dy \quad (2f)$$

$$B_1 \equiv \frac{\omega_{m1}^2 n_{m1}^2 n_{n1}^2}{4c^2 k_{n1}\cos\theta_{n1}} \left\{P_1S_1\int_0^\infty U_{m1}U_{n1}U_{a1}\,dy + r_1E_{p1} \cdot \int_0^\infty U_{m1}U_{n1}U_{p1}\,dy\right\} \Big/ \int_{-\infty}^\infty U_{n1}^2\,dy \quad (2g)$$

and

p_1 relevant photoelastic constant or constants,
r_1 relevant electrooptic coefficient or coefficients,
c velocity of light in free space,
$\Delta\theta_1$ deviation of incident angle from Bragg angle.

It is to be noted that the input boundary values to an adjacent SAW in the case with multiple tilted SAW's are simply those given by (2c) and (2d) with appropriate phase factors added to account for the propagation delay between the two SAW's.

B. Diffraction Efficiency

From (2c)–(2g), the diffraction efficiency which is the ratio of the diffracted light power at the output ($x = L_1$) and the incident light power at the input of the interaction region ($x = 0$) can be found:

$$\zeta_1 = g_1^2 \left\{ \frac{\sin\left[g_1^2 + (K_1 \Delta\theta_1 L_1/2)^2\right]^{1/2}}{\left[g_1^2 + (K_1 \Delta\theta_1 L_1/2)^2\right]^{1/2}} \right\}^2 \tag{3a}$$

where

$$g_1^2 \equiv A_1 B_1 L_1^2 = \left(\frac{\pi^2}{4\lambda_0^2}\right)(n_{m1}^3 n_{n1}^3 \Gamma_{m1n1}^2 L_1^2/\cos\theta_{m1}\theta_{n1}) \tag{3b}$$

$$\Gamma_{m1n1}^2 = \left\{ \int_0^\infty U_{m1} U_{n1} (P_1 S_1 U_{a1} + r_1 E_{p1} U_{p1})\, dy \right\}^2 \Bigg/ \left\{ \int_{-\infty}^\infty U_{m1}^2\, dy \right\} \left\{ \int_{-\infty}^\infty U_{n1}^2\, dy \right\} \tag{3c}$$

and λ_0 is wavelength of the incident light wave in free space, and L_1 is aperture of the SAW.

From (3a), it is seen that the diffraction efficiency is a sensitive function of Γ_{m1n1}^2, the so-called overlap integral [14], and also that dependence on the material parameters differs drastically from that in bulk-type AO interactions [9]. An efficient diffraction can occur only when the confinement of the undiffracted and diffracted light waves matches the penetration depth of the SAW.

Finally, the relationship between the parameter g_1^2 and the total acoustic power P_{A1} is shown to be

$$P_{A1} \cong -\tfrac{1}{2} L_1 \int_0^\infty \mathrm{Re}\,\{(V_x + V_y + V_z)^* \cdot (-e_1 E_{p1} U_{p1} + c_1 S_1 U_{a1})\}\, dy \tag{3d}$$

$$g_1^2 \cong -\left(\frac{\pi^2}{2\lambda_0^2}\right)\left(\frac{n_{m1}^3 n_{n1}^3 L_1}{\cos\theta_{m1}\cos\theta_{n1}}\right) \cdot \left(\frac{1}{\int_0^\infty \mathrm{Re}\,\{F_x + V_y + V_z)^* (-e_1 E_{p1} U_{p1} + c_1 S_1 U_{a1})\}\, dy} \right) \cdot \Gamma_{m1n1}^2 P_{A1} \tag{3e}$$

where Re designates the fact that only the real part is to be taken; e_1 and c_1 are, respectively, the relevant piezoelectric and stiffness constants; and V_x, V_y, and V_z designate the relevant displacement velocities. It is to be noted that in (3d) the piezoelectric contribution to the acoustic power is neglected as it is small compared with the strain contribution.

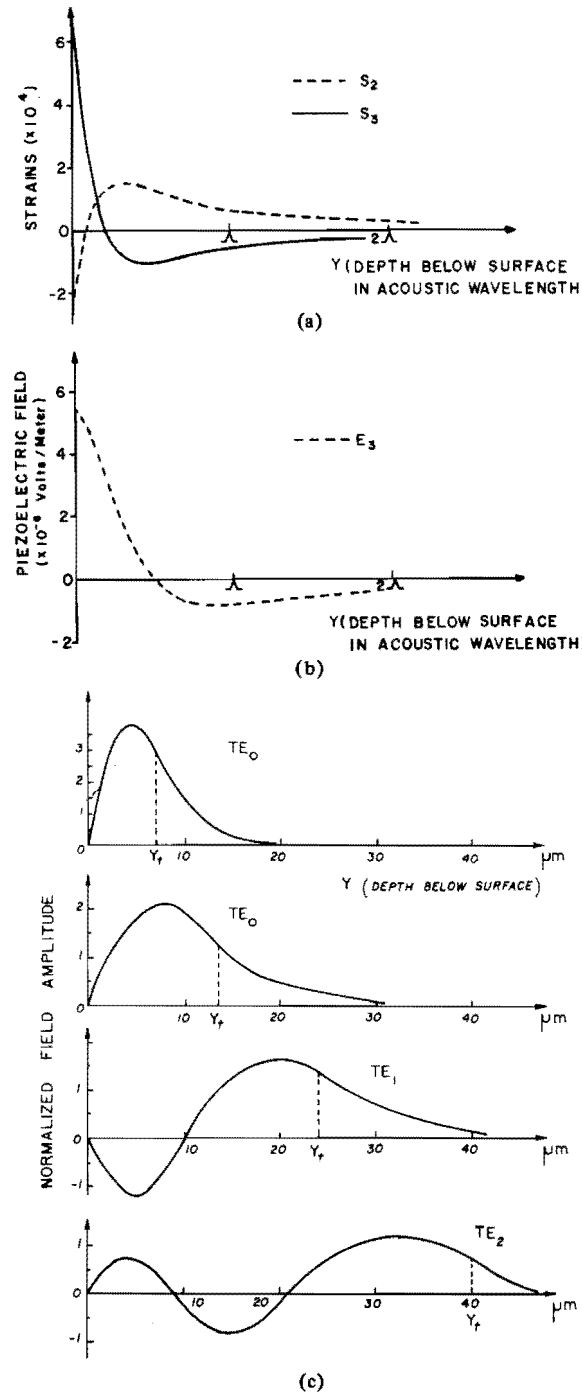

Fig. 3. (a) Depth dependence of the strain fields for the SAW propagating along the z axis of Y-cut $LiNbO_3$ substrate. (b) Depth dependence of the accompanying piezoelectric fields to (a). (c) Profiles of TE optical waveguide modes in Y-cut $LiNbO_3$ out-diffused layers (Y_t is the turning point).

For the case with the SAW propagating in either the z direction or 21.8° from the z axis of a Y-cut $LiNbO_3$ substrate, with which experiments have been carried out (Section IV), all relevant parameters are known [15], [16]. Thus the relative contributions to the diffraction due to the elastooptic and electrooptic effects (3c), as well as the relationship between P_{A1} and g_1^2 (3e), can be calculated numerically.

Numerical calculation of the relative elastooptic and electrooptic contributions to the diffraction has been carried out for the case of He–Ne laser light (0.6328 μm) propagating in a Y-

cut $LiNbO_3$ out-diffused optical guiding layer. The relevant SAW propagation parameters are taken from [16]. For example, the depth dependence of the strains of the z-propagating SAW and the accompanying piezoelectric field have been calculated using these parameters and are given in Fig. 3(a) and (b), respectively. Note that the penetration depth of the SAW is inversely proportional to the acoustic frequency. It is assumed in this calculation that both the diffracted and the undiffracted light waves belong to the same TE mode, namely, $n_{m1} = n_{n1}$. This assumption is based on the fact that no mode conversion has been observed in the experiments to be described later. The normalized optical field distribution $U_{m1}(y)$ or $U_{n1}(y)$ for the three lowest order modes is regenerated from the formulation given in [17], as shown in Fig. 3(c).

Finally, the relevant photoelastic constants and electrooptic coefficients are needed for the numerical calculation of (3c). For the SAW propagating along or approximately along the $z(c)$ axis of the Y-cut $LiNbO_3$ substrate, the dominant strain components responsible for the interaction are S_2 and S_3 with the corresponding photoelastic constants $P_{31} = P_{32} = 0.178$ and $P_{33} = 0.088$ [18]. The corresponding electrooptic coefficients are $r_{33} = 31 \times 10^{-10}$ V/cm and $r_{31} = r_{32} = 0$. It can be shown that for the SAW propagating along or approximately along $\pm 21.8^\circ$ from the $z(c)$ axis, five components of the strain fields and two components of the associated electric field contribute to the diffraction. The two dominant strain components are S_5 and S_6 with the corresponding photoelastic constants $(-0.38P_{14}) = -0.06$ and $(-0.048P_{11} - 0.297P_{31} + 0.048P_{13} + 0.297P_{33}) = 0.024$. The dominant electric field component is E_1 with the corresponding electrooptic coefficient $(0.128r_{13} + 0.8r_{33} + 0.256r_{42}) = 32.9 \times 10^{-10}$ V/cm.

Using the acoustic and optical field distributions and the elastrooptic and electrooptic parameters as described above, spatial variations of the relative elastooptic and electrooptic contributions to the Bragg diffraction have been calculated. The results are shown in Fig. 4. It is to be noted that Fig. 4(a) agrees with [4, fig. 2]. From Fig. 4(a) and (b) it is seen that while the electrooptic effect is the dominant cause of the diffraction in the case of the z-propagating SAW, both the electrooptic and the elastooptic effects contribute nearly equally to the diffraction for the case of the 21.8°-propagating SAW. Similarly, the relative Bragg diffraction efficiency as a function of the acoustic frequency, with the penetration depth of the waveguide mode as a parameter, can also be calculated. Fig. 5 presents the calculated results for the two directions of propagation using a SAW of 1.74-mm aperture and an optical TE_0 mode of two penetration depths. These plots clearly show that the z-propagating SAW can provide more efficient Bragg diffraction at relatively low acoustic frequency. In contrast, the 21.8°-propagating SAW provides more efficient Bragg diffraction at higher acoustic frequency. Furthermore, the smaller the penetration depth of the optical guiding layer, the higher will be the diffraction efficiency and the operating frequency. Consequently, the 21.8°-propagating SAW was employed in the devices to be described in Section IV.

C. Bandwidth Limitations

From (3a) it can also be seen that the interaction bandwidth, assuming a sufficiently large acoustic bandwidth, depends not only on the acoustic aperture L_1 but also on g_1^2, and thus the diffraction efficiency. This is because the penetration depth of the SAW, and thus $\Gamma m1n1^2$, varies with the acoustic frequency. In the following analysis, the -3-dB interaction bandwidth $2\Delta f_1$ is calculated for the case with center frequency f_{01}. Since at the exact Bragg condition ($\Delta\theta_1 = 0$) and at $f_1 = f_{01}$ the diffraction efficiency is given by $\{\sin g_1(f_{01})\}^2$, the half-bandwidth Δf_1 can be determined from the following equality:

$$\frac{1}{\sqrt{2}} \cdot \frac{\sin f_1(f_{01})}{g_1(f_{01} \pm \Delta f_1)} \cong \frac{\sin [g_1^2(f_{01} \pm \Delta f_1) + \{\pi(f_{01} \pm \Delta f_1)\Delta\theta_1 L_1/v_{R1}\}^2]^{1/2}}{[g_1^2(f_{01} \pm \Delta f_1) + \{\pi(f_{01} \pm \Delta f_1)\Delta\theta_1 L_1/v_{R1}\}^2]^{1/2}} \quad (4a)$$

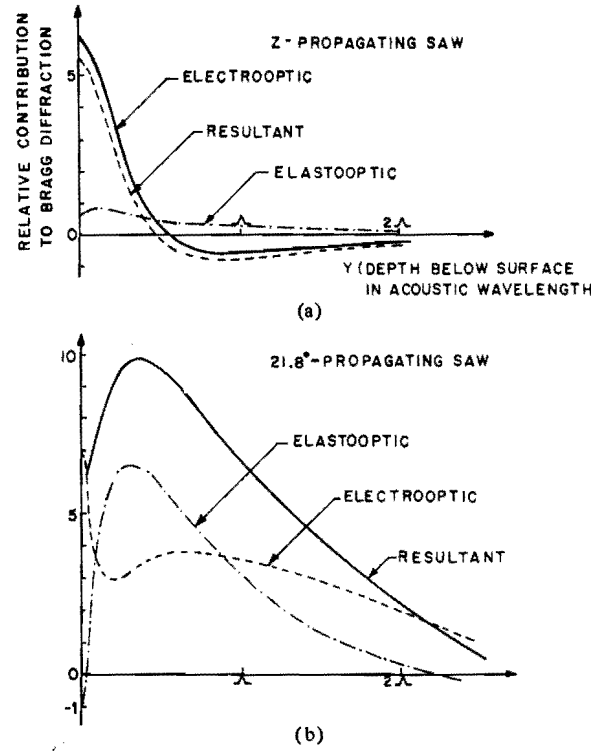

Fig. 4. Depth dependence of relative elastooptic and electrooptic contributions to Bragg diffraction. (a) For z-propagating SAW. (b) For 21.8°-propagating SAW.

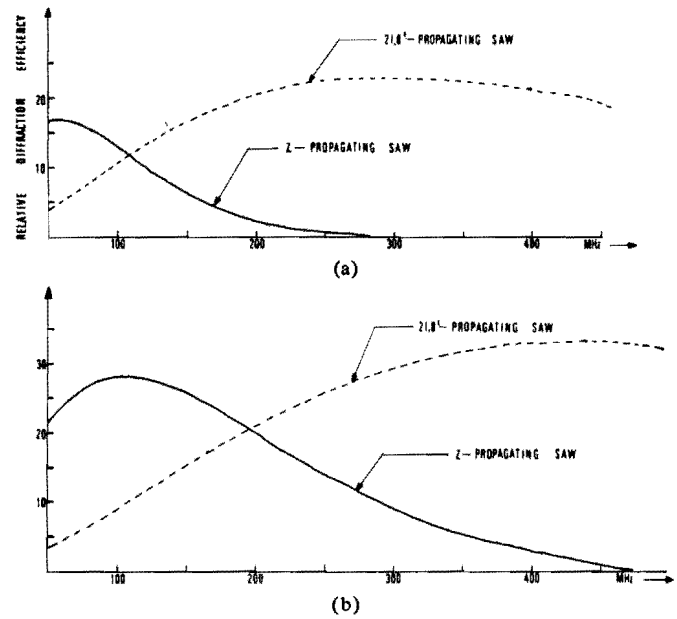

Fig. 5. Relative Bragg diffraction efficiency versus acoustic frequency in Y-cut $LiNbO_3$ out-diffused waveguides. (a) Penetration depth of TE_0 mode = 13.5 μm. (b) Penetration depth of TE_0 mode = 7.0 μm.

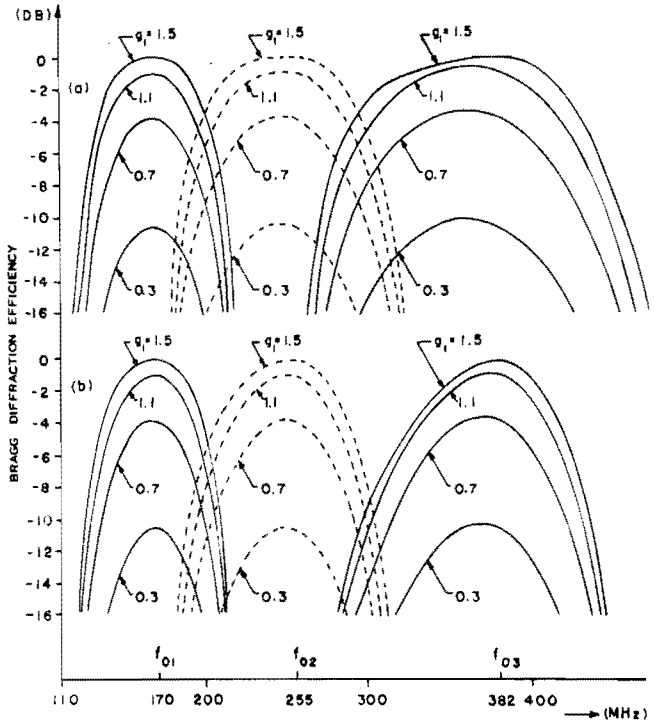

Fig. 6. Frequency response of guided-wave acoustooptic Bragg diffraction from a single SAW. (a) $L_1 = 2.5$ mm, $L_2 = 1.66$ mm, and $L_3 = 1.11$ mm. (b) $L_1 = 5.0$ mm, $L_2 = 3.32$ mm, and $L_3 = 2.22$ mm. (The 21.8°-propagating SAW gives almost identical frequency response as the z-propagating SAW.)

where

$$\Delta\theta_1 = \frac{\lambda_0}{2n_{m1}v_{R1}\cos\theta_{m1}}\left[1 - \{(n_{m1}^2 - n_{n1}^2)v_{R1}^2/f_{01}^2\lambda_0^2\}\right]\Delta f_1 \tag{4b}$$

or

$$\Delta\theta_1 = \frac{\lambda_0}{2n_{m1}v_{R1}\cos\theta_{m1}}\Delta f_1, \quad \text{for } n_{m1} = n_{n1} \tag{4c}$$

and v_{R1} designates the velocity of the SAW.

Again, using the acoustic and optical field distributions and the elastooptic and electrooptic parameters described previously, a set of frequency response curves for the lowest order TE mode (TE_0), having g_1 as a parameter, have been obtained and are shown in Fig. 6. In these plots, the acoustic waves are assumed to have center frequencies of 170, 255, and 382 MHz, each with a 30-percent fractional acoustic bandwidth Δf_a. Fig. 6(a) is plotted for the acoustic apertures $L_1 = 2.5$ mm, $L_2 = 1.66$ mm, and $L_3 = 1.11$ mm; Fig. 6(b) is plotted for acoustic apertures 100-percent larger. It is seen that the interaction bandwidth decreases as the acoustic aperture increases and may become smaller than the acoustic bandwidth at large acoustic aperture. For example, a Bragg bandwidth of only 45 MHz is possible for a device using a Y-cut $LiNbO_3$ outdiffused waveguide of 7-μm penetration depth in which the acoustic aperture is 0.5 cm and the acoustic center frequency is 380 MHz.

From the analytical and numerical results presented above, we may conclude that the bandwidth of the guided-wave AO Bragg devices using a single SAW not only is limited by the acoustic center frequency, the acoustic bandwidth, and the aperture of the SAW, but also depends on the diffraction efficiency and the optical modes involved. For the devices which employ the TE_0 and/or TE_1 modes, the device bandwidth increases slightly as the diffraction efficiency increases. For other optical modes, the device bandwidth may decrease as the diffraction efficiency increases. It is observed that for a device which utilizes a single SAW of low acoustic center frequency, the absolute device bandwidth is mainly limited by the acoustic bandwidth. On the other hand, for a device which employs a single SAW of high acoustic center frequency, the absolute device bandwidth is mainly limited by the Bragg bandwidth. Thus the diffraction efficiency-bandwidth product of a device using a single SAW is rather limited. However, it is clear that by employing a number of SAW's which are of staggered center frequency and tilted propagation direction, efficient Bragg diffraction in each frequency band will make it possible to achieve a large composite bandwidth, and thus a large diffraction efficiency-bandwidth product.

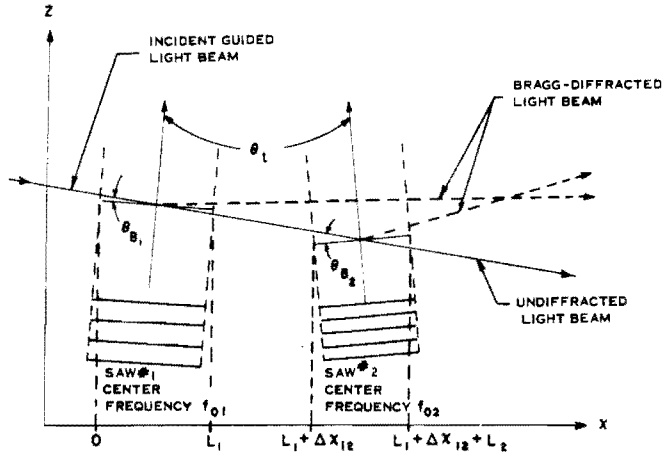

Fig. 7. Guided-wave acoustooptic Bragg diffraction from two tilted SAW's.

III. Acoustooptic Bragg Diffraction from Two Tilted Surface Acoustic Waves

As mentioned in the beginning of Section II, the input boundary values (the diffracted and undiffracted light fields) for the interaction region of the second SAW are obtained by adding a phase factor, which accounts for the propagation delay between the two adjacent SAW's, to (2c) and (2d). Thus the methodology for numerical computation which has been developed for the case involving a single SAW can be conveniently extended to the case involving multiple tilted SAW's. For simplicity, only the case with two tilted SAW's (Fig. 7) is treated in this paper. Note that in Fig. 7 the tilt angle θ_t between the two SAW's is set equal to the difference in the Bragg angles at the two acoustic center frequencies. We shall first calculate the resultant diffraction efficiency for this case.

For convenience we shall express the boundary values at the input edge of the second SAW as follows:

$$E_{m2}(L_1 + \Delta x_{12}) = \alpha \tag{5a}$$

$$E_{n2}(L_1 + \Delta x_{12}) = \beta \exp(j\varphi) \tag{5b}$$

where from (2) and (3) we have

$$\alpha = (1 - \zeta_1)^{1/2} \tag{5c}$$

$$\beta = (\zeta_1)^{1/2} \tag{5d}$$

$$\varphi = \pi/2 + (K_1\Delta\theta_1\Delta x_{12}/2) + \tan^{-1}\{(K_1\Delta\theta_1/2q_1) \cdot \sin(q_1L_1)/\cos(q_1L_1)\} + \phi_1 \tag{5e}$$

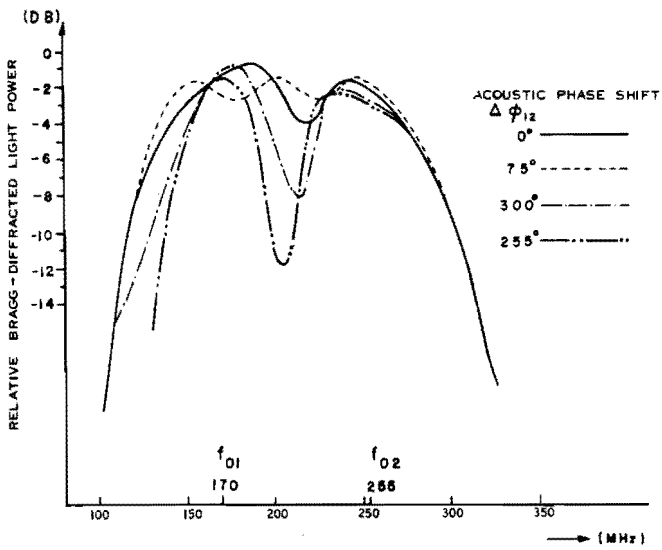

Fig. 8. Effect of phase shift between two tilted SAW's on resultant frequency response (theoretical).

where φ designates the relative phase between the undiffracted and the diffracted light waves and includes the phase shift ϕ_1 of the first SAW. Substituting (5) into the general solutions for $E_{m2}(x)$ and $E_{n2}(x)$, which take the same form as $E_{m1}(x)$ and $E_{n1}(x)$, we obtain the electric fields of the diffracted light wave at the output of the interaction region:

$$E_{n2}(L_1 + \Delta x_{12} + L_2) = [\beta \cos(q_2 L_2) + j(1/q_2) \cdot \{(K_2 \Delta\theta_2/2)\beta + \alpha B_2 \exp j(\phi_2 - \varphi)\} \cdot \sin q_2 L_2] \times \exp j\{-(K_2 \Delta\theta_2 L_2/2) + \varphi\} \quad (6)$$

where K_2, ϕ_2, $\Delta\theta_2$, L_2, q_2, and B_2 are defined in the same manner as those in the first SAW.

In order to calculate the resultant diffraction efficiency ζ_T, we first note that the diffraction efficiency ζ_1 due to the first SAW is simply $|\beta \exp(j\varphi)|^2$, which is given by (3a). We also note that the diffraction efficiency ζ_2 due to the second SAW alone is given by $(B_2^2/q_2^2) \sin^2 q_2 L_2$ because $A_2 = B_2$. Thus the resultant diffraction efficiency, which is simply $|E_{n2}(L_1 + \Delta x_{12} + L_2)|^2$, is

$$\zeta_T = \zeta_1(1 - \zeta_2) + \zeta_2(1 - \zeta_1) + 2\{\zeta_1(1 - \zeta_1)\zeta_2\}^{1/2}\{(K_2 \Delta\theta_2/2q_2) \cdot \sin q_2 L_2 \cos(\phi_2 - \varphi) - \cos q_2 L_2 \sin(\phi_2 - \varphi)\}. \quad (7)$$

From (7), it is seen that $\zeta_T \approx \zeta_1$ for the frequency range $f_a \leqslant f_{01}$ and $\zeta_T \approx \zeta_2$ for the frequency range $f_a \geqslant f_{02}$. On the contrary, for the frequency range $f_{01} \leqslant f_a \leqslant f_{02}$, both acoustic waves contribute to the diffraction and the resultant diffraction efficiency is given by the sum of three terms. The effect of the interference between the two acoustic waves on the resultant diffraction efficiency is represented by the cross term. It is clear that enhancement as well as reduction in the diffraction efficiency occurs as the phase shift $(\phi_2 - \varphi)$ varies.

Using (7), a family of plots have been generated for the diffraction efficiency versus the acoustic frequency, with the phase shift between the two SAW's $\Delta\phi_{12}$ as a parameter. Some sample plots for a He-Ne laser light are shown in Fig. 8. In order to compare these calculated plots with the measured ones to be shown in Section IV, the acoustic and the acousto-optic parameters for these plots are chosen to be identical to those used in Section IV—namely, f_{01} = 170 MHz, f_{02} = 255 MHz, L_1 = 2.5 mm, and L_2 = 1.66 mm—and the tilt angle set equal to the difference in the corresponding Bragg angles at the center frequency for the individual SAW's—namely, 3.4 mrad. From the plots it is seen that the phase shift may cause destructive as well as constructive interference in the resultant diffracted light power. Consequently, the resultant (composite) bandwidth can be larger than the sum of the two individual bandwidths. Therefore, the phase shift as well as the tilt angle between adjacent SAW's are the important parameters, in addition to the center frequency and the acoustic aperture of the individual SAW's, for the design of wide-band high-diffraction efficiency Bragg devices.

In summary, the analysis and the methodology for the numerical calculation described above for the case involving two tilted SAW's may be extended to the case involving more than two tilted SAW's, and it can be concluded that by using multiple SAW's, which are staggered in their center frequency and tilted in their propagation direction, guided-wave AO Bragg devices with large diffraction efficiency-bandwidth product can be realized.

IV. Experimental Results

A Y-cut $LiNbO_3$ substrate possesses an attractive combination of acoustic, piezoelectric, optical, acoustooptic, and electrooptic properties [19], [20]. In addition, an optical waveguiding layer may be easily created on the top of the substrate using a number of fabrication techniques. Thus a number of multiple tilted transducers (the transducer axes were at 21.8° from the $z(c)$ axis) have been fabricated on such substrates to study the wide-band technique discussed above. The waveguiding layers were grown using the out-diffusion technique [12] and the interdigital transducers were fabricated using the well-established photolithographic method [21].

A. Design of the Tilted SAW Transducers

Two versions of the tilted SAW transducers, namely, three- and four-element transducers, were fabricated and employed in the experimental study. The center frequencies of the three-element transducers are 170, 255, and 382 MHz, with the corresponding acoustic apertures of 2.5, 1.66, and 1.11 mm, respectively, and the tilt angles between adjacent transducers are 3.4 and 5.2 mrad, corresponding to the difference in the Bragg angles at the center frequency of the adjacent transducers. In order to obtain as wide an acoustic bandwidth as possible, the number of finger electrode pairs for each transducer was chosen to be as small as two and a half. The measured acoustic bandwidths of approximately 30 percent of the center frequencies, namely, 50, 68, and 115 MHz, were obtained by inserting a single inductance of proper value to each transducer. The acoustic wavelengths at the center frequency are 20.5, 13.7, and 9.3 μm, respectively. This version of tilted transducers was used to study the frequency response, as well as the effect of phase shift on the frequency response, and the electric drive power requirement.

The center frequencies of the four-element transducers are 140, 220, 290, and 400 MHz, with the corresponding apertures of 2.2, 2.2, 1.6, and 1.1 mm, respectively, and the tilt angles between the adjacent transducers are 2.5, 3.5, and 5.0 mrad, respectively. The number of finger electrode pairs for each transducer was chosen to be two, with the measured acoustic bandwidths of approximately 35 percent of the center frequencies, namely, 45, 69, 90, and 150 MHz. Finally, the acoustic wavelengths at the center frequencies are 23.5, 16.4, 11.6, and 8.1 μm, respectively.

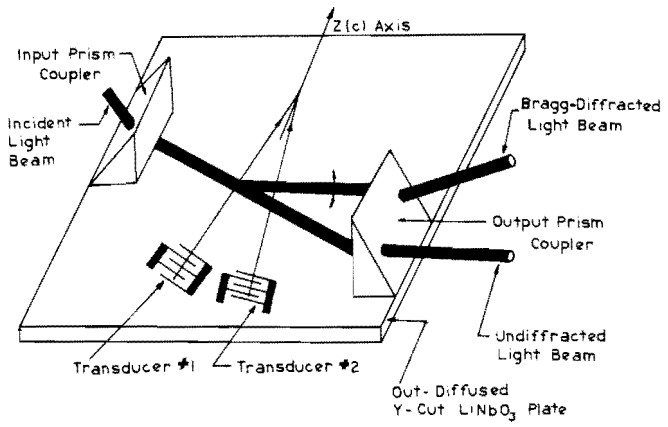

(a)

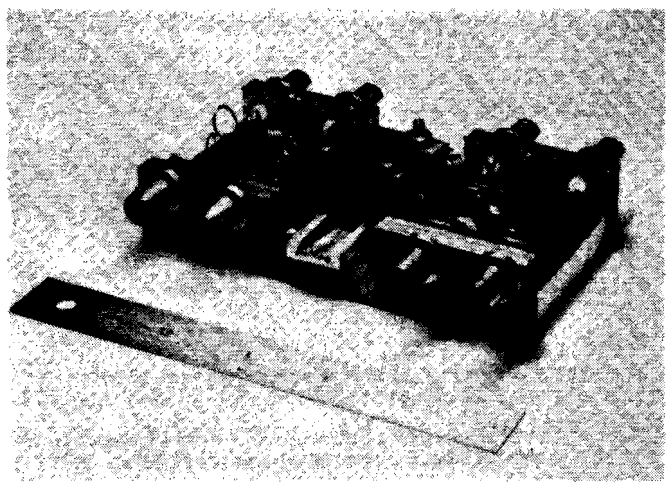

(b)

Fig. 9. (a) Experimental configuration for guided-wave acoustooptic Bragg diffraction. (b) Guided-wave AO deflector using multiple tilted SAW's.

B. Optical Waveguide, Optical Beam, and Acoustooptic Parameters

A He–Ne laser light at 0.6328 μm was utilized in the experiments. A rutile prism was used to couple an unguided light beam into a guided light beam with the polarization approximately along 21.8° from the c axis of the $LiNbO_3$, and a second rutile prism was used to couple out both the diffracted and the undiffracted light beams (Fig. 9(a)). A photograph of one of the units used in this study is shown in Fig. 9(b). Note that the prism couplers and the $LiNbO_3$ crystal are located in the middle of the brass plate. The out-diffused waveguide supports a single TE mode, namely, TE_0, with a penetration depth of approximately 7 μm. The corresponding maximum change of refractive index at the surface is estimated to be approximately 5×10^{-4}. The best throughput coupling efficiency is as high as 25 percent. The aperture of the guided light beam can be varied from 1 to 6 mm, with a slight degradation in the uniformity of the light beam for the widest aperture. The variation of the throughput coupling efficiency as a function of the diffraction spread of the incident light beam, which ranges from 1 to 16 mrad, was measured to be only two to one.

The Q parameters (defined as $2\pi\lambda_0 L/n\Lambda^2$) are 11, 16, and 24, respectively, for the three-element version. Thus Bragg diffraction prevails in all frequency bands. Since the Q parameters for the four-element version are 6.5, 13.1, 19.2, and 27, respectively, Bragg diffraction also prevails in all frequency bands.

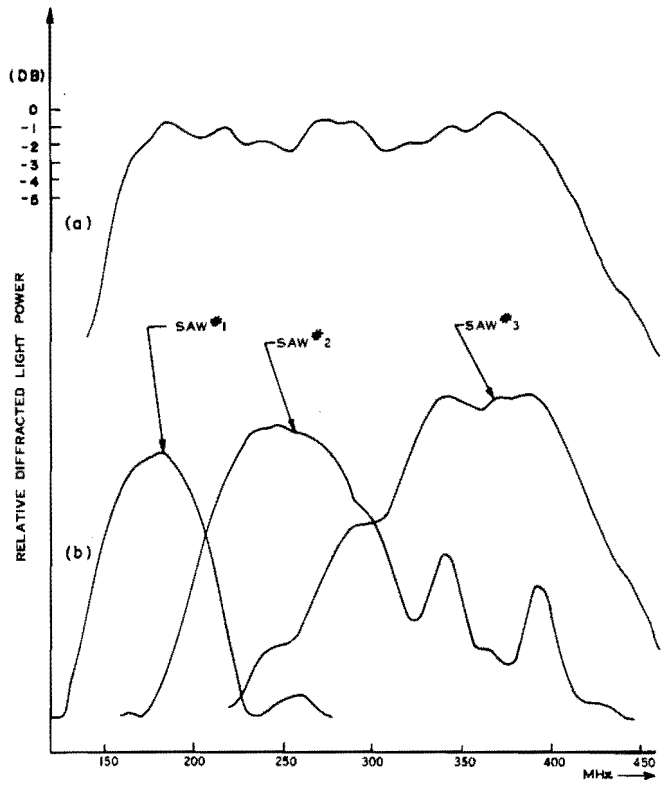

Fig. 10. Frequency responses of Bragg-diffracted light power. (a) For three combined SAW's. (b) For individual SAW's.

C. Frequency Responses and Electric Drive Power Requirement

The individual transducers were excited in parallel using power dividers, and the phase shifts between adjacent SAW's were implemented by using sections of coaxial cables. The incident angle of the guided light beam was adjusted, by using a precision holder for the device, to optimize for both the diffraction efficiency and the resultant bandwidth. Fig. 10 shows the recorder plots of the resultant frequency response from the three-element tilted SAW's together with those from the individual SAW's. It is seen that the device has a -3-dB resultant bandwidth of approximately 245 MHz while the bandwidths using the individual SAW's are 45, 65, and 82 MHz, respectively. Clearly, the resultant bandwidth is larger than the sum of the three individual bandwidths. The source for the two weak satellite peaks in the frequency response of SAW #2 is not clear at this point. The allowable variation of the incident angle of the light beam (outside the crystal) to maintain the same bandwidth is approximately 0.5°. Typical diffraction efficiency versus the total electric drive power at the center frequency is shown in Fig. 11. It is seen that a total electric drive power of 220 mW is required to diffract 50 percent of the incident light. The corresponding total acoustic power is estimated to be at most 15 mW because the best conversion efficiency of the transducers was measured to be -13 dB. Based on the above performance figures, the diffraction efficiency-bandwidth product of this particular device is substantially larger than previous devices [9].

The frequency response for the four-element tilted SAW's device is shown in Fig. 12. Clearly, a -3-dB resultant bandwidth of 358 MHz has been realized in this unit. Measurements of the device bandwidth and the diffraction efficiency as a function of the diffraction spread of the incident light beam indicate that they do not vary more than a factor of

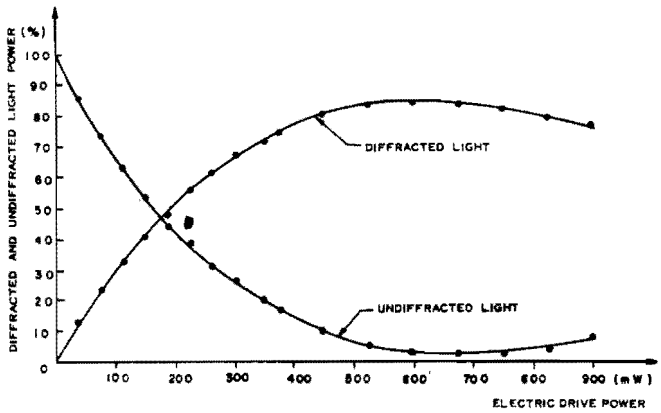

Fig. 11. Percentage diffracted and undiffracted light power versus total electric drive power.

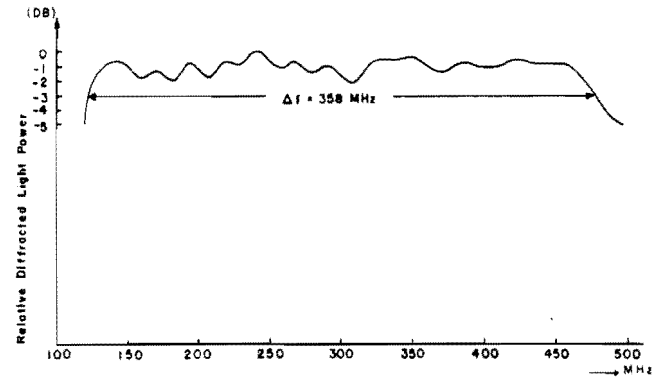

Fig. 12. Resultant frequency response of Bragg-diffracted light power from four tilted SAW's.

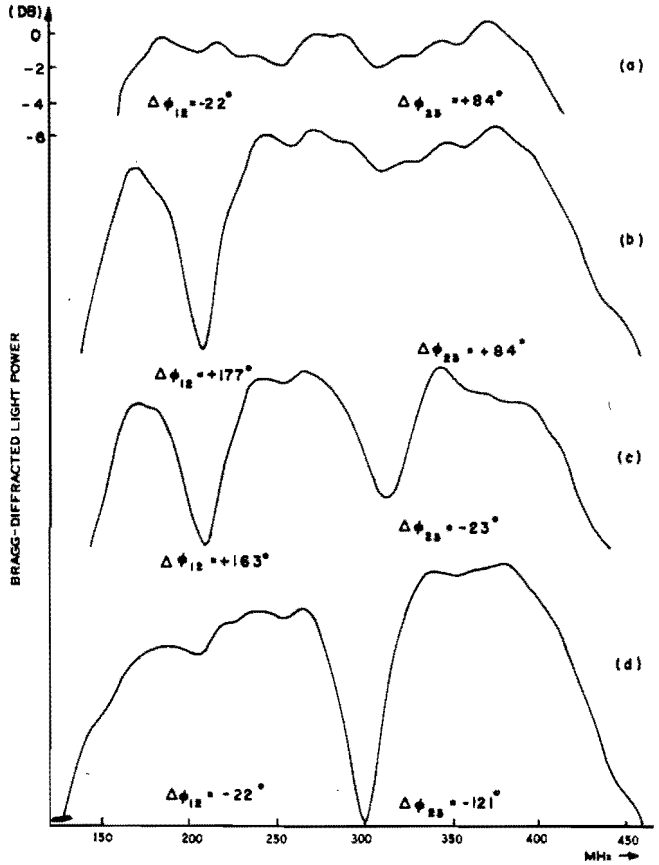

Fig. 13. Effect of electric phase shift between adjacent transducers on resultant frequency response (experimental).

two for the range of diffraction spread mentioned previously. Although a detailed measurement of the diffraction efficiency versus the electric drive power had not been made for this unit before it was damaged, an earlier measurement had indicated that the electric drive power required was two to three times larger than that of the unit with three-element tilted SAW's.

D. Effect of the Phase Shift Between Adjacent Transducers on the Resultant Frequency Response

As mentioned previously, interference between adjacent SAW's becomes important in the range of frequencies at which both adjacent transducers excite SAW's efficiently. This interference will in turn affect the diffraction efficiency, and thus the resultant frequency response. Fig. 13 illustrates this interference effect in the frequency band around 210 MHz and 310 MHz for the unit with three-element transducers. It is apparent that as the electric phase shift $\Delta\phi_{12}$ was varied from -22° (Fig. 13(a)) to $+177^\circ$ (Fig. 13(b)), the diffraction efficiency varied by a factor of -11 dB. Similarly, when the electric phase shift $\Delta\phi_{23}$ was varied from $+84^\circ$ (Fig. 13(a)) to -121° (Fig. 13(d)), the diffraction efficiency varied by a factor of -14 dB. It is to be noted that although it is difficult to compare the theoretical results with the experimental results based on the absolute phase shift (since in the experiments the phase shift was implemented electrically, while in the analysis the phase shift is assumed to be that between the adjacent SAW's), the effect of the phase shift as predicted in the analysis (Fig. 8) has been clearly demonstrated in the experiments (Fig. 13). Fig. 13 has clearly demonstrated that the resultant frequency response of the devices which employ multiple tilted SAW's can be made flat by inserting appropriate phase shifters between adjacent transducers. Also, in doing so, the resultant device bandwidth may be made larger than the sum of the individual bandwidths [2d].

E. Beam Profile and Number of Resolvable Spot Diameters

The optical waveguiding layers utilized in the devices being studied support the lowest order TE mode. No mode conversion between the diffracted and undiffracted light beams was observed. Fig. 14(a) shows the undeflected light spot (when no RF power was applied to the device) and Fig. 14(b) shows the deflected light spots, both at the far field, for the unit with three-element transducers as the frequency of the driving signal was varied from 155 to 410 MHz. The aperture of the incident light beam employed is approximately 0.1 cm. It is observed that the quality of the undeflected light beam (RF power off) is preserved in the deflected light beam, and that deflected light beams of satisfactory quality are achievable.

In beam deflection and switching applications, the number of resolvable beam diameters N is given by

$$N = \left(\frac{D}{V_R}\right)\Delta f = \tau\Delta f \tag{8}$$

where D designates the aperture of the light beam, V_R the velocity of the SAW, Δf the device bandwidth, and τ the transit time of the SAW across the incident light beam aperture. (The transit time may be practically defined as the switching time of the device if the time response of the electric drive circuit is sufficiently faster than the transit time.) Clearly, for a fixed device configuration, a large N can be achieved by having a large D and/or a large Δf. However, a

(a) (b)

Fig. 14. Far-field undeflected and deflected light beams. (a) Undeflected light beam with RF power off. (b) Deflected light beam positions as the frequency of the drive signal was varied from 155 to 410 MHz at 15 MHz per step.

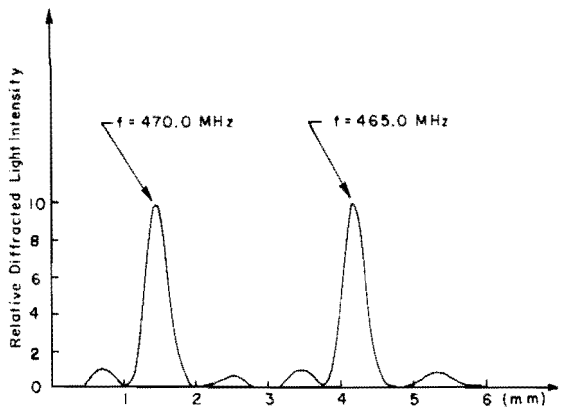

Fig. 15. Beam profile of deflected light at two acoustic frequencies.

large D necessarily implies a large transit time and, therefore, a slower switching speed. In addition, as a result of the acoustic attenuation and/or the waveguide imperfection, a large D will cause some degradation in the beam quality of the deflected light, and thus some reduction in N. Therefore, it is more desirable to achieve a large N through a large Δf rather than a large D.

In the various units that have been studied, the maximum D obtainable was approximately 0.6 cm with some breakage into filaments in the middle of the light beam. However, a uniform beam of approximately 0.45 cm is achievable with the unit which has a 358-MHz bandwidth. Using 3.5×10^5 cm/s for V_R, we predicted from (8) that the incremental frequency change required for deflection of one Rayleigh spot diameter ($N = 1$) is $\delta f \simeq 0.78$ MHz. The measured value as determined from the plots of the deflected light beam profiles (Fig. 15) along the direction of deflection, as recorded by a fiber optic probe, is approximately 0.8 MHz. This close match between calculated and measured values indicates that the quality of the deflected light beam is not degraded appreciably by the diffraction process—in agreement with the beam quality illustrated in Fig. 14. Since the total bandwidth of this device, Δf, is 358 MHz, the device can deflect a light beam of 0.45-cm aperture into 400 Rayleigh spot diameters at a random-access switching time of 1.28 μs.

If the aperture of the light beam is enlarged to 1 cm, the light beam can be deflected by the same device into 1000 Rayleigh spot diameters at a random-access switching time of 2.8 μs. Equivalently, the same device is capable of switching a guided light beam of 95-μm aperture into 10 beam positions (channels) at a switching time of 27 ns. A 1-cm aperture should be achievable either by improving the surface condition of both the prism couplers and the $LiNbO_3$ plate and/or the contact between them, or by using grating couplers [22].

V. Conclusion

The results of theoretical and experimental studies have shown that very wide-band high-efficiency guided-wave AO Bragg devices can be realized by employing multiple SAW's which are staggered in their operating frequency and tilted in their propagation direction. Relevant parameters as well as important considerations for the design of such wide-band devices have been established. Based on the experimental results achieved so far, the devices have provided the best combination of performance figures—namely, RF drive power requirements, device bandwidth, and random-access switching time—among the existing acoustooptic devices. It should be possible to achieve even better performance figures when an in-diffused or a step-index waveguide of smaller optical confinement is used, instead of a gradient-index waveguide such as the out-diffused waveguides employed in this study. A waveguide structure which consists of a thin step-index layer of As_2S_3 (or other AO material of larger figure of merit) deposited on a $LiNbO_3$ substrate [1] can also provide better performance figures than those provided by the $LiNbO_3$ out-diffused waveguides.

The development of the wide-band technique presented in this paper has made it possible to design and fabricate very wide-band guided-wave AO Bragg devices, and has thus paved the way for a number of potential applications using such devices. Possible wide-band applications, in addition to those common to bulk-type AO devices, include processing (convolution, correlation, etc.) of wide-band RF signals [23], high-speed optical pulse modulation, AO spectrum analysis of very wide-band RF signals [2d], [24], high-speed multiport beam switching, and deflection for fiber/integrated optic systems [2d], [24]. These applications have been demonstrated experimentally and the detailed results will be reported in a future paper.

Acknowledgment

The authors wish to thank Dr. A. G. Milnes and Dr. D. L. Feucht for allowing them to use the solid-state facilities for the work presented in this paper.

References

[1] Y. Ohmachi, "Acousto-optical light diffraction in thin films," *J. Appl. Phys.*, vol. 44, p. 3928, Sept. 1973.

[2] a) C. S. Tsai and Le T. Nguyen, "Surface acoustic wave array transducers and their applications," in *Proc. Optical and Acoustical Microelectronics*. New York: Polytechnic Press, 1974, vol. XXIII, p. 583.

b) C. S. Tsai, S. K. Yao, and M. A. Alhaider, "High performance guided-wave acoustooptic deflection using multiple surface acoustic waves," presented at the Integrated Optics and Fiber Optics Communication Conf., NELC, San Diego, CA, May 1974, Post-Deadline Paper D.12 (unpublished).

c) C. S. Tsai, Le T. Nguyen, S. K. Yao, and M. A. Alhaider, "High performance acoustooptic guided-light-beam device using two

tilting surface acoustic waves," *Appl. Phys. Lett.*, vol. 26, p. 140, Feb. 1975.
C. S. Tsai, Le T. Nguyen, and M. A. Alhaider, "A wideband acoustooptic guided-light beam deflector using tilting surface acoustic waves," in *Proc. 1974 IEEE Ultrasonics Symp.* (IEEE Cat. 74 CHO-896-ISU), pp. 768-772.
d) C. S. Tsai, M. A. Alhaider, Le T. Nguyen, and B. Kim, "Wideband guided-wave acoustooptic Bragg devices using multiple tilting surface acoustic waves," presented at the IEEE/OSA Conf. Laser Engineering and Applications, Washington, DC, May 1975; *Dig. Tech. Papers*, p. 10.

[3] K. W. Loh, W. S. C. Chang, W. R. Smith, and T. Grudkowski, "Bragg coupling efficiency for guided acoustooptic interaction in GaAs," to be published in *Appl. Opt.*

[4] J. M. White, P. F. Heidrich, and E. G. Lean, "Thin-film acoustooptic interaction in $LiNbO_3$," *Electron. Lett.*, vol. 10, p. 510, Nov. 28, 1974.

[5] R. V. Schmidt and I. P. Kaminow, "Acoustooptic Bragg deflection in $LiNbO_3$ Ti-diffused waveguides," *IEEE J. Quantum Electron.* (Corresp.), vol. QE-11, pp. 57-59, Jan. 1975.

[6] Earlier references on guided-wave acoustooptic interactions are given in [2c]. See also N. Chubachi, J. Kushibiki, and Y. Kikuchi, "Monolithically integrated Bragg deflector for an optical guided wave made of zinc-oxide film" *Electron. Lett.*, vol. 9, pp. 193-194, 1973.

[7] NSF Workshop on Acoustical Microelectronics, Stanford Univ., Stanford, CA, Nov. 7, 1973.

[8] W. R. Smith, H. M. Gerard, J. H. Collins, T. M. Reeder, and H. J. Shaw, "Design of surface wave delay lines with interdigital transducers," *IEEE Trans. Microwave Theory Tech.*, vol. MTT-17, pp. 865-873, Nov. 1969.

[9] C. F. Quate, C. D. W. Wilkinson, and D. K. Winslow, "Interaction of light and microwave sound," *Proc. IEEE*, vol. 53, pp. 1604-1623, Oct. 1965.
E. I. Gordon, "A review of acoustooptical deflection and modulation devices," *Appl. Opt.*, vol. 5, p. 1629, Oct. 1966.
N. Uchida and N. Niizeki, "Acoustooptic deflection materials and techniques," *Proc. IEEE*, vol. 61, pp. 1073-1092, Aug. 1973.

[10] a) A. Korpel, R. Alder, P. Desmares, and W. Watson, "A television display using acoustic deflection and modulation of coherent light," *Proc. IEEE*, vol. 54, pp. 1429-1437, Oct. 1966.
G. A. Coquin, J. P. Griffin, and L. K. Anderson, "Wide-band acoustooptic deflectors using acoustic beam steering," *IEEE Trans. Sonics Ultrason.*, vol. SU-17, pp. 34-40, Jan. 1970.
D. A. Pinnow, "Acousto-optic light deflection: Design considerations for first order beam steering transducers," *IEEE Trans. Sonics Ultrason.*, vol. SU-18, pp. 209-214, Oct. 1971.
b) R. M. de la Rue, C. Steward, C. D. W. Wilkinson, and I. R. Williamson, "Frequency-controlled beam steering of surface acoustic waves using a stepped transducer array," *Electon. Lett.*, vol. 8, p. 326, July 1973.

[11] C. S. Tsai, B. Kim, and Le T. Nguyen, "Wideband guided-wave acoustooptic Bragg diffraction using phased-surface acoustic wave array in $LiNbO_3$ waveguides," presented at the Ultrasonics Symp., Los Angeles, CA, Sept. 1975; *Symp. Dig.*, pp. 42-43. To be published in *Proc. IEEE (Special Issue on Surface Acoustic Waves)*, May 1976.

[12] I. P. Kaminow and J. R. Carruthers, "Optical waveguiding layers in $LiNbO_3$ and $LiTaO_3$," *Appl. Phys. Lett.*, vol. 22, p. 326, 1973.
N. F. Hartman, R. P. Kenan, P. R. Sievert, C. M. Verber, and V. E. Wood, "Characteristics of diffused waveguiding layers in $LiNbO_3$," presented at the Integrated Optics Meeting, New Orleans, LA, Jan. 1974.

[13] R. W. Dixon, "Acoustic diffraction of light in anisotropic media," *IEEE J. Quantum Electron.*, vol. QE-3, pp. 85-93, Feb. 1967.

[14] L. Kuhn, M. L. Dakss, P. F. Heidrich, and B. A. Scott, "Deflection of an optical guided wave by a surface acoustic wave," *Appl. Phys. Lett.*, vol. 17, p. 265, Sept. 1970.

[15] *Microwave Acoustics Handbook*, vol. 1A, *Surface Wave Velocities*, A. J. Slobodnik, E. D. Conway, and R. T. Delmonico, Eds., under AFCRL-TR-73-0597, Oct. 1, 1973.

[16] R. N. Spaight and G. G. Koerber, "Piezoelectric surface waves on $LiNbO_3$," *IEEE Trans. Sonics Ultrason.*, vol. SU-18, pp. 237-238, Oct. 1971.

[17] D. Marcuse, "TE modes of graded-index slab waveguides," *IEEE J. Quantum Electron.*, vol. QE-9, pp. 1000-1006, Oct. 1973.

[18] R. W. Dixon and M. G. Cohen, "A new technique for measuring magnitudes of photoelastic tensors and its application to lithium niobate," *Appl. Phys. Lett.*, vol. 8, p. 205, Apr. 1966.

[19] C. S. Tsai, Le T. Nguyen, and P. Saunier, "New guided wave acoustooptic and electrooptic devices using $LiNbO_3$," presented at the IEEE Symp. Applications of Ferroelectrics, Albuquerque, NM, June 1975; *Symp. Dig.*, pp. 78-79.

[20] C. S. Tsai and P. Saunier, "Ultrafast guided-light beam deflection/switching and modulation using simulated electrooptic prism structures in $LiNbO_3$ waveguides," *Appl. Phys. Lett.*, vol. 27, p. 248, Aug. 1975.

[21] H. I. Smith, F. J. Bachner, and N. Efremow, "A high-yield photolithographic technique for surface wave devices," *J. Electrochem. Soc.*, vol. 118, p. 821, May 1971.

[22] M. L. Dakss, L. Kuhn, P. F. Heidrich, and B. A. Scott, "Grating coupler for efficient excitation of optical guided waves in thin films," *Appl. Phys. Lett.*, vol. 16, p. 523, June 15, 1970.

[23] C. S. Tsai, "Wideband guided-wave acoustooptic Bragg devices and applications," in *Proc. 1975 IEEE Ultrasonics Symp.* (IEEE Cat. 75 CHO-994-4SU), pp. 120-125.

[24] M. C. Hamilton, D. A. Wille, N. F. Hartman, C. M. Verber, and R. P. Kenan, "Acoustooptic diffraction in $LiNbO_3$ waveguides," in *Proc. 1974 Electrooptic Systems Design Conf.* (Industrial and Scientific Conf. Management, Chicago, IL), p. 174.
D. L. Hecht, "Broadband acoustooptic spectrum analysis," in *Proc. 1973 IEEE Ultrasonics Symp.*, p. 98.